# Use Sentinel Satellite Data for Estimation of Soil Properties: A Review

Prajakta Labade[1*], D.N. Jagtap[2], Unnati R. Sonawane[3], Pooja. P.Thul[4], B.L.Ayare[5]

[*1]Ph.D Scholar, Department of Soil and Water Conservation Engineering, CAET, DBSKKV, Dapoli, Maharashtra, India
[2]Assistant Professor, Department of Agronomy, COA, DBSKKV, Dapoli, Maharashtra, India
[3]Ph.D Scholar, Department of Soil and Water Conservation Engineering, CAET, DBSKKV, Dapoli, Maharashtra, India
[4]Ph.D Scholar, Department of Process and Food Engineering, CAET, DBSKKV, Dapoli, Maharashtra, India
[5]Professor and Head, Department of Soil and Water Conservation Engineering, CAET, DBSKKV, Dapoli, Maharashtra, India.
*Corresponding Author

Received:- 10 October 2024/ Revised:- 19 October 2024/ Accepted:- 23 October 2024/ Published: 31-10-2024


***Abstract*****—** *Soils are an important component of the critical zone and a finite resource. Mapping and monitoring these resources in the field, regional, and global stages is crucial for better management and prevention of degradation. Remote sensing (RS) techniques provide several advantages over conventional approaches for evaluating soil parameters, including large-scale coverage, non-destructive nature, temporal monitoring, multispectral capabilities, and rapid data collecting. Aside from laboratory circumstances, Sentinel satellite data has been used to estimate various soil parameters in a variety of applications. This review highlights research on soil properties estimation using sentinel data, including methodology and outcomes for each study. Various soil properties like Soil Texture, Soil Salinity, Soil Texture, Soil Organic Carbon estimated using sentinel data.*

***Keywords— Soil, Sentinel, Satellite, Properties.***

## I. INTRODUCTION

Accurate information, needed to managing the variability in soil properties, is an important aspect in the implementation of site-specific farming also known as precision agriculture (PA) (Jarosalv et al., 2018). In agricultural fields, soil properties often show relevant spatial variations (Yuzugullu et al., 2020) due to several factors, e.g., parent material, geomorphology, previous use, and management. The primary method for the characterization of soil involves manually collecting soil samples, drying them, and subsequently performing chemical analyses in a laboratory setting (Toth et al., 2013). However, the manual collection of soil samples, along with their corresponding physicochemical characterization, is a time-consuming process that lacks scalability for extensive areas (Wang et al., 2014). Different soil properties interact with electromagnetic radiation in diverse ways. As electromagnetic waves strike the Earth's surface, they can be absorbed, transmitted, or reflected. The reflection and absorption patterns at different wavelengths provide insights into the composition, structure, and properties of the observed materials (Barnes et al., 2000). More recently, hyperspectral, and multispectral soil characterization has emerged as a highly valuable tool for the estimation of soil properties without the need for chemical analyses of the soil samples (Lagacherie et al., 2008 and Helfer et al., 2021). Another approach is given by multispectral satellite sensors. Since 1972, Landsat satellites gather images that can be useful in environmental studies. For example, sensor thematic mapper (TM) on-board Landsat 5 was used to detect bare soil (Dematte et al. 2009). In 2015, the European Space Agency (ESA) begin to deliver free of cost, good spatial resolution (10 m) Earth images. Sensors on-board optical Sentinel-2 satellites are equipped with 12 spectral bands, which can be useful for soil properties mapping. The usefulness of the acquired image data largely depends on the way it is processed and analysed. Many statistical methods are used to obtain reliable soil information from multispectral images, such as multiple linear regression (MLR) analysis, principal component regression (PCR) and partial least squares (PLS) regression. Application of the latter method to hyperspectral data allows to determine several soil parameters with high values of correlation coefficient and low errors, including grain size composition, pH, cation exchange capacity (CEC) or some chemical elements (Mammadov et al. 2020, Vestergaard et al. 2021). Recently, machine learning algorithms based on random

forests and Cubist development models have been used to study the relationship between spectral data and soil characteristics. The Cubist model is often used to estimate SOC; in such cases, it is also advisable to use spectral indices as variables in addition to raw reflectance (Peng et al. 2015). More precisely, which soil parameters, with what method of data analysis and with what accuracy, can be estimated based on satellite data.

## II. A REVIEW ON VARIOUS SOIL PROPERTIES ESTIMATION USING SENTINEL SATELLITE IMAGES

### 2.1 Soil Moisture:

Qi et al used use of Sentinel-1 and Sentinel-2 data for soil moisture mapping at 100 m resolution. This paper presents two methodologies for the retrieval of soil moisture from remotely-sensed SAR images, with a spatial resolution of 100 m. These algorithms are based on the interpretation of Sentinel-1 data recorded in the VV polarization, which is combined with Sentinel-2 optical data for the analysis of vegetation effects over a site in Urgell (Catalunya, Spain). The first algorithm has already been applied to observations in West Africa by Zribi et al., 2008, using low spatial resolution ERS scatterometer data, and is based on change detection approach. In the present study, this approach is applied to Sentinel-1 data and optimizes the inversion process by taking advantage of the high repeat frequency of the Sentinel observations. The second algorithm relies on a new method, based on the difference between backscattered Sentinel-1 radar signals observed on two consecutive days, expressed as a function of NDVI optical index. Both methods are applied to almost 1.5 years of satellite data (July 2015–November 2016), and are validated using field data acquired at a study site. This leads to an RMS error in volumetric moisture of approximately 0.087 $m^3/m^3$ and 0.059 $m^3/m^3$ for the first and second methods, respectively. No site calibrations are needed with these techniques, and they can be applied to any vegetation-covered area for which time series of SAR data have been recorded.

Paloscia et al studied soil moisture mapping using Sentinel-1 images. The main objective of this research is to develop, test and validate a soil moisture content (SMC) algorithm for GMES Sentinel-1 characteristics. The SMC product, which is to be generated from Sentinel-1 data, requires an algorithm capable of processing operationally in near-real-time and delivering the product to the GMES services within 3 h from observation. An approach based on an Artificial Neural Network (ANN) has been proposed that represents a good compromise between retrieval accuracy and processing time, thus enabling compliance with the timeliness requirements. The algorithm has been tested and subsequently validated in several test areas in Italy, Australia, and Spain. In all cases the validation results were very much in line with GMES requirements (with RMSE generally 4%SMC – between 1.67% SMC and 6.68% SMC – and very low bias), except for the case of the test area in Spain, where the validation results were penalized by the availability of only VV polarized SAR images and MODIS low-resolution NDVI. Nonetheless, the obtained RMSE was slightly higher than 4%SMC.

Figure 1 Histogram of the comparison between the ANN-estimated and the ground measured SMC over the Cordevole area. SMC was subdivided into 4 classes between 25% and 45%. Two ANNs were considered: one used only VV polarized data, and the other one also used the NDVI information.

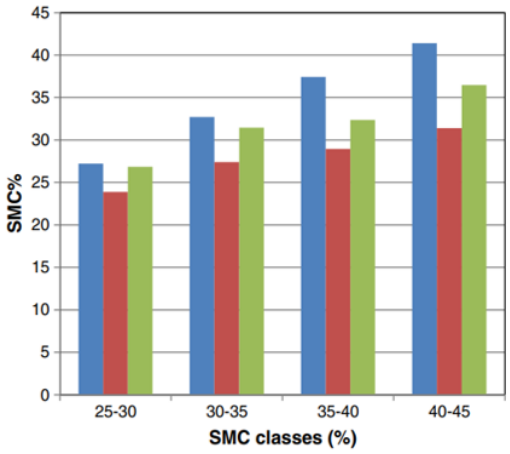


**FIGURE 1: Histogram of SMC Comparison Between ANN-Estimated and Ground Measured Values**

Table 1 Validation results, obtained over the test site in Spain, by considering (a) or disregarding (b) NDVI information. In grey, the couples of values SMC estimated/SMC measured, for which the NDVI information worsened the results, have been singled out.

**TABLE 1**
**VALIDATION RESULTS FOR ANN-ESTIMATED SMC WITH AND WITHOUT NDVI INFORMATION**

| Part A | | | | |
|---|---|---|---|---|
| **Acquisition date** | **SMC ANN (%)** | **SMC ground (%)** | **RMSE (%)** | **St. Dev. (%)** |
| 10 May, 2010 | 16.11 | 24.05 | 5.34 | 3.45 |
| 14 June, 2010 | 12.66 | 14.35 | 3.52 | 2.66 |
| 23 August, 2010 | 10.18 | 7.86 | 3.41 | 2.19 |
| 27 September, 2010 | 17.19 | 14.99 | 6.38 | 4.76 |
| 25 February, 2011 | 13.74 | 21.41 | 4.58 | 0.69 |
| 22 June, 2011 | 11.58 | 10.85 | 4.35 | 3.44 |
| Mean | | | 4.6 | 2.87 |
| **Part B** | | | | |
| 10 May, 2010 | 20.06 | 24.05 | 2.72 | 0.97 |
| 14 June, 2010 | 16.37 | 14.34 | 4.01 | 2.69 |
| 23 August, 2010 | 16.65 | 7.85 | 8.5 | 2.9 |
| 27 September, 2010 | 17.92 | 14.99 | 5.12 | 3.23 |
| 25 February, 2011 | 20.31 | 21.4 | 2.31 | 0.58 |
| 22 June, 2011 | 16.39 | 10.85 | 5.21 | 1.71 |
| Mean | | | 4.64 | 2.01 |

Natalia et conducted study on soil moisture estimation using Sentinel-1/-2 Imagery coupled with cycleGAN for Time-series Gap Filing This study aimed to explore the possibility of taking advantage of freely available Sentinel-1 (S1) and Sentinel-2 (S2) EO data for the simultaneous prediction of SMC with cycle-consistent adversarial network (cycleGAN) for time-series gap filling. The proposed methodology, first, learns latent low-dimensional representation of the satellite images, then learns a simple machine learning model on top of these representations. To evaluate the methodology, a series of vineyards, located in South Australia's Eden valley are chosen. Specifically, we presented an efficient framework for extracting latent features from S1 and S2 imagery. They showed how one could use S1 to S2 feature translation based on Cycle-GAN using S1and S2 time series when there are missing images acquired over an area of interest. The resulting data in our study is then used to fill gaps in time series data. We used the resulting latent representations to predict SMC with various ML tools. In the experiments, cycleGAN and the autoencoders were trained with data randomly chosen around the site of interest, so we could augment the existing dataset. The best performance was demonstrated with random forest algorithm, whereas linear regression model demonstrated significant overfitting. The experiments demonstrate that the proposed methodology outperforms the compared state-of-the-art methods if there are missing optical and synthetic-aperture radar (SAR) images.

Figure 2 Proposed architecture relies on building a latent representation of each domain (S1 and S2) based on autoencoders and then predicting Soil Moisture (through an additional prediction model) based on these representations. A cycleGAN is also trained to recover missing data from S1 to S2 and vice-versa.

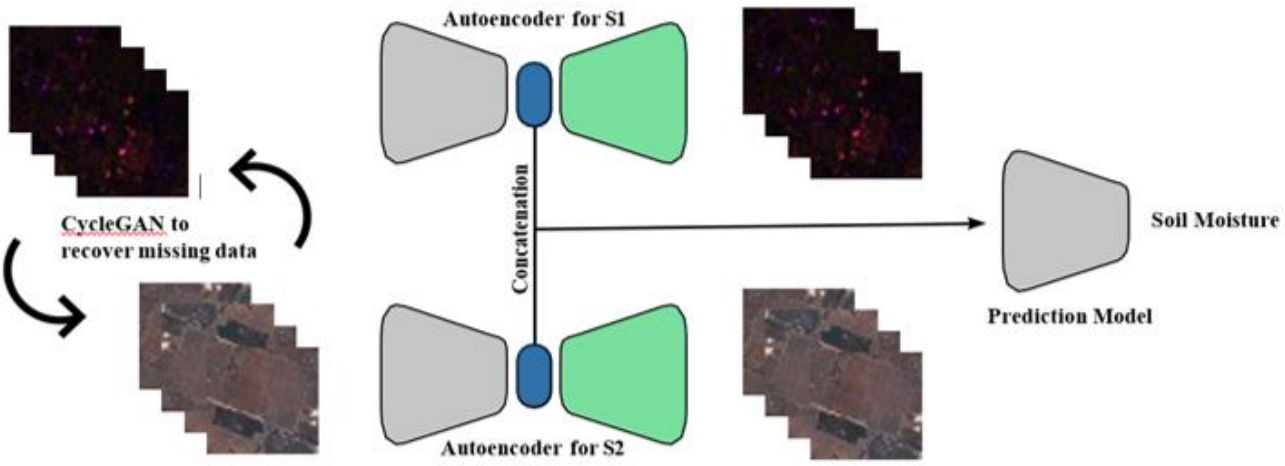


**FIGURE 2: Proposed Architecture for Cross-Domain Soil Moisture Prediction**

Sutariya et al presents the potential for soil moisture (SM) retrieval using Sentinel-1 C-band Synthetic Aperture Radar (SAR) data acquired in Interferometric Wide Swath (IW) mode along with Land Surface Temperature (LST) estimated from analysis of LANDSAT-8 digital thermal data. In this study Sentinel-1 data acquired on 27 February 2020 was downloaded from Copernicus website and LANDSAT-8 OLI data acquired on 24 February 2020 from the website https://earthexplorer.usgs.gov/.The soil samples were collected from 70 test fields in different villages of three talukas for estimating soil moisture content using the gravimetric method. The Sentinel-1 SAR microwave data was analysed using open-source tools of Sentinel Application Platform (SNAP) software for estimation of backscattering coefficient. Land surface temperature estimated using Landsat-8 thermal data. The Landsat8, Thermal infrared sensor Band-10 data and operational land imager Band-4 and Band-5 data were used in estimating LST. The Soil Moisture Index (SMI) for all field test sites was computed using the LST values. The regression analysis using σ0VV and σ0VH polarization with soil moisture indicated that σ0VV polarization was more sensitive to soil moisture content as compared to σ0VH polarization. The multiple regression analysis using field measured soil moisture (MS %) as dependent variable, and σ0VV and SMI as independent variable was carried which resulted in the coefficient of determination ($R^2$) of 0.788, 0.777 and 0.778 for Godhra, Gogh amba and Kalol talukas, respectively. These linear regression equations were used to compute the predicted soil moisture in three talukas.

Esmaeili et al estimated of soil moisture using sentinel-1 and sentinel-2 images. For this study, soil moisture was sampled at 24 points in the common area of the two images in the south of Malard city, Tehran province (Iran) was obtained by survey. After pre-processing the images, the values of bands 1 to 7, 11, and 12 of the Sentinel-2 and applying filters (Gaussian, Laplacian, Majority, Morphology, and rank) to the Sentinel-1 soil moisture were calculated. Moreover, R, $R^2$, and RMSE were calculated using soil moisture obtained from sample points. Furthermore, Maps of data used by sentinel-1 and sentinel-2 images were obtained. Using maps of data shows the potential of applied filters to sentinel-1 and bands used for sentinel-2 in the estimation of soil moisture. According to the results, the highest coefficient of determination ($R^2$) for the Sentinel-2 is related to band 6 with 84%. The result of Sentinel-1 demonstrated that the highest coefficient of determination was related to the Rank filter (54%). The highest correlation of the Sentinel-2 and the Sentinel-1 is related to band 6 with 74% and the Rank filter with 46%, respectively. The lowest RMSE in Sentinel-2 and Sentinel-1 is related to band three (1.64 %) and rank filter (1.03 %), respectively. According to the obtained results, band 6 in the Sentinel-2 and filter in Sentinel-1 have better performance among the data and methods used. However, it is emphasized that using more samples can be tested for improving results.

**TABLE 2**

**CORRELATION AND RMSE RESULTS BETWEEN INPUT DATA AND SOIL MOISTURE**

| Data | RMSE | R | Soil Moisture Values (% ) |
|---|---|---|---|
| B1 | 11.42 | 0.13 | 8.7 |
| B2 | 3.68 | 0.2 | 8.09 |
| B3 | 1.64 | 0.306 | 7.93 |
| B4 | 6.16 | 0.315 | 8.29 |
| B5 | 4.5 | 0.67 | 8.16 |
| B6 | 3.68 | 0.74 | 8.097 |
| B7 | 3.67 | 0.369 | 8.096 |
| B8 | 2.26 | 0.415 | 7.98 |
| B11 | 4.4 | 0.16 | 8.15 |
| B12 | 4.88 | 0.19 | 8.19 |
| Sentinel-1 | 4.92 | 0.18 | 8.19 |
| Gaussian | 11.34 | 0.15 | 8.69 |
| Laplacian | 14.29 | 0.068 | 8.92 |
| Major | 2.36 | 0.069 | 7.99 |
| Rank | 1.03 | 0.46 | 7.89 |
| Morphology | 6.67 | 0.13 | 8.33 |

### 2.2 Soil Organic Carbon and Soil Organic Matter:

Castaldi et al assessed the capability of Sentinel-2 time-series to estimate soil organic carbon and clay content at local scale in croplands. This work is focused on the feasibility of Sentinel-2 based approaches for the high-resolution mapping of topsoil clay and organic carbon (SOC) contents at the within-farm or within-field scales, for cropland sites of contrasted climates and soil types across the Northern hemisphere. Four pixelwise temporal mosaicking methods, using a two years-Sentinel-2 time series and several spectral indices (NDVI, NBR2, BSI, S2WI), were developed and compared for i) pure bare soil condition (maxBSI), ii) driest soil condition (minS2WI), iii) average bare soil condition (Median) and iv) dry soil conditions excluding extreme reflectance values (R90). Three spectral modelling approaches, using the Sentinel-2 bands of the output temporal mosaics as covariates, were tested, and compared: (i) Quantile Regression Forest (QRF) algorithm; (ii) QRF adding longitude and latitude as covariates (QRFxy); (iii) a hybrid approach, Linear Mixed Effect Model (LMEM), that includes spatial autocorrelation of the soil properties. We tested pairs of mosaic and spectral approaches on ten sites in Türkiye, Italy, Lithuania, and USA where soil samples were collected and SOC and clay content were measured in the lab. The average RPIQ of the best performances among the test sites was 2.50 both for SOC (RMSE = 0.15%) and clay (RMSE = 3.3%). Both accuracy level and uncertainty were mainly influenced by site characteristics of cloud frequency, soil types and management. Generally, the models including a spatial component (QRFxy and LMEM) were the best performing, while the best spatial mosaicking approaches mostly were Median and R90. The most frequent optimal combination of mosaicking and model type was Median or R90 and QRFxy for SOC, and R90 and LMEM for clay estimation.

**TABLE 3**
**FREQUENCY OF ACCURACY VALUES HIGHER THAN 90% FOR SOC ESTIMATION AMONG THE TEN TEST SITES ACCORDING TO SYNTHETIC BARE SOIL IMAGES METHOD (SBSI) AND PREDICTION MODELS.**

| | maxBSI | minS2WI | Median | R90 | Mean frequency |
|---|---|---|---|---|---|
| **QRF** | 10% | 50% | 40% | 50% | 37.50% |
| **QRFxy** | 40% | 50% | 60% | 60% | 52.50% |
| **LMM** | 30% | 40% | 30% | 50% | 37.50% |
| **Mean frequency** | 26.70% | 46.70% | 43.30% | 53.30% | |

Castaldi et al investigated soil organic carbon mapping using LUCAS Topsoil database and Sentinel-2 Data: An approach to reduce soil moisture and crop residue effects. In this regard, the high temporal, spatial, and spectral resolution of the Sentinel-2 data can be exploited for monitoring SOC contents in the topsoil of croplands. In this study, we aim to test the effect of the threshold for a spectral index linked to soil moisture and crop residues on the performance of SOC prediction models using the Multi-Spectral Instrument (MSI) Sentinel-2 and the European Land Use/cover Area frame Statistical survey (LUCAS) topsoil database. The LUCAS spectral data resampled according to MSI/Sentinel-2 bands, which were used to build SOC prediction models combining pairs of the bands. The SOC models were applied to a Sentinel-2 image acquired in North-Eastern Germany after removing the pixels characterized by clouds and green vegetation. Then, we tested different thresholds of the Normalized Burn Ratio 2 (NBR2) index in order to mask moist soil pixels and those with dry vegetation and crop residues. The model accuracy was tested on an independent validation database and the best ratio of performance to deviation (RPD) was obtained using the average between bands B6 and B5 (Red-Edge Carbon Index: RE-CI) (RPD: 4.4) and between B4 and B5 (Red-Red-Edge Carbon Index: RRE-CI) (RPD: 2.9) for a very low NBR2 threshold (0.05). Employing a higher NBR2 tolerance (higher NBR2 values), the mapped area increases to the detriment of the validation accuracy. The proposed approach allowed us to accurately map SOC over a large area exploiting the LUCAS spectral library and, thus, avoid a new ad hoc field campaign. Moreover, the threshold for selecting the bare soil pixels can be tuned, according to the goal of the survey. The quality of the SOC map for each tolerance level can be judged based on the figures of merit of the model.

Madugundu et al studied estimation soil organic carbon in agricultural fields: A remote sensing approach. Landsat-8 (L8) and Sentinel-2 (S2A) satellite images were used for the characterization of SOC stocks in the topsoil layer (0-10 cm) of the experimental fields. Soil samples were randomly collected from six (50 ha each) agricultural fields and analysed in the laboratory for SOC (SOC) following Walkley and Black A method. While, vegetation indices (VI), such as the Normalized Difference Vegetation Index (NDVI), NDVIRedEdge, Enhanced Vegetation Index (EVI), Bare Soil Index (BSI), and Reduced Simple Ratio (RSR) were computed and subsequently used for the development of SOC prediction models. Univariate linear regression technique was employed for the recognition of a suitable band/VI for SOC (SOC) mapping. The SWIR-1 P2 band of both L8 ($R^2$ = 0.86) and S2A (R=0.77) data was promising for predicting SOC with 16% (S2A) and 18% (L8) of BIAS.

Xinxin et al estimated soil organic matter content using sentinel-2 imagery by machine learning in Shanghai. This article aimed to evaluate the capacity of Sentinel-2 for SOM prediction in an urban area (i.e., Shanghai). 103 bare soil samples filtrated from 398 soil samples at a depth of 20 cm were selected. Three methods, partial least square regression (PLSR), artificial neural network (ANN), and support vector machine (SVM), were applied. The root mean square error (RMSE) of modelling (mRMSE) and the coefficient of determination ($R^2$) of modelling ($mR^2$) were used to reflect the accuracy of the model. The results show that PLSR has the poorest performance. ANN has the highest modelling accuracy (mRMSE = 7.387 g $kg^{-1}$, $mR^2$ = 0.446). The ANN prediction accuracy of RMSE (pRMSE) is 4.713 g $kg^{-1}$ and the prediction accuracy of $R^2$ ($pR^2$) is 0.723. For SVR, the pRMSE is 4.638 g $kg^{-1}$, and the $pR^2$ is 0.732. The prediction accuracy of SVR is slightly higher than that of ANN. The spatial distribution of SOM demonstrates that the value obtained by ANN is the closest to the range of the bare soil samples, and ANN performs better in vegetation-covered areas. Therefore, Sentinel-2 can be used to estimate SOM content in urban areas, and ANN is a promising method for SOM estimation.

**TABLE 4**
**ACCURACY EVALUATION OF MODEL AND PREDICTION ACCURACY**

| Method | Modelling Accuracy | | Prediction Accuracy | |
|---|---|---|---|---|
| | $mR^2$ | mRMSE | $pR^2$ | pRMSE |
| ANN | 0.446 | 7.387 | 0.723 | 4.713 |
| SVR | 0.256 | 8.556 | 0.732 | 4.638 |
| PLSR | 0.155 | 9.12 | 0.349 | 7.224 |

Klara et al presented study on have collected 303 photos of soil surfaces in the Belgian loam belt where five main classes of surface conditions were distinguished: smooth seeded soils, soil crusts, partial cover by a growing crop, moist soils, and crop residue cover. Reflectance spectra were then extracted from the Sentinel–2 images coinciding with the date of the photos. After the growing crop was removed by an NDVI < 0.25, the Normalized Burn Ratio ($NBR^2$) was calculated to characterize the soil surface, and a threshold of $NBR^2$ < 0.05 was found to be able to separate dry bare soils from soils in unfavourable conditions i.e. wet soils and soils covered by crop residues. Additionally, we found that normalizing the spectra (i.e. dividing the reflectance of each band by the mean reflectance of all spectral bands) allows for cancelling the albedo shift between soil crusts and smooth soils in seed–bed conditions. They then built the exposed soil composite from Sentinel–2 imagery for southern Belgium and part of Noord Holland and Flevoland in the Netherlands (covering the spring periods of 2016–2021). They used the mean spectra per pixel to predict SOC content by means of a Partial Least Squares Regression Model (PLSR) with 10–fold cross–validation. The uncertainty of the models was assessed via the prediction interval ratio (PIR). The cross validation of the model gave satisfactory results (mean of 100 bootstraps: model efficiency coefficient (MEC) = 0.48 ± 0.07, RMSE = 3.5 ± 0.3 g C $kg^{-1}$, RPD = 1.4 ± 0.1 and RPIQ = 1.9 ± 0.3). The resulting SOC prediction maps show that the uncertainty of prediction decreases when the number of scenes per pixel increases, and reaches a minimum when at least six scenes per pixel are used. The results of a validation against an independent data set showed a median difference between the measured (average SOC content 13.5 g C $kg^{-1}$) and predicted SOC contents at field scale. Overall, this compositing method shows both realistic within field and regional SOC patterns.

**TABLE 5**
**STATISTICS OF THE SOIL ORGANIC CARBON (SOC) CONTENT PREDICTION AND THE UNCERTAINTY (%) FOR THE PIXEL–BASED APPROACH AND FOR FIELD–BASED APPROACH. (SD = STANDARD DEVIATION)**

| Approach | N | | Mean | Median | SD |
|---|---|---|---|---|---|
| Per-Pixel | 11, 235, 492 pixels | SOC (g C $kg^{-1}$) | 14.1 | 13.3 | 4.7 |
| | | PIR (g C $kg^{-1}$) Per–field | 12.4 | 11.8 | 1.6 |
| Per-Field | 92, 451 fields | SOC (g C $kg^{-1}$) | 13.6 | 12.7 | 3.2 |
| | Validation (n=34 385 | Residues (g C $kg^{-1}$) | 0.7 | 0.5 | 2.8 |

Chong et al mapped soil organic matter content using Sentinel-2 synthetic images at different time intervals in Northeast China. In this study, they processed all Sentinel-2 images covering the bare-soil period (March to June) in Northeast China from 2019 to 2022 and integrated the observation results into synthetic materials with four defined time intervals (10, 15, 20, and 30 d). Then, they used synthetic images corresponding to different time periods to conduct SOM mapping and determine the optimal time interval and time period before finally assessing the impacts of adding environmental covariates. The results showed the following: (1) in SOM mapping, the highest accuracy was obtained using day-of-year (DOY) 120 to 140 synthetic images with 20 d time intervals, as well as with different time intervals, ranked as follows: 20 d > 30 d > 15 d > 10 d; (2) when using synthetic images at different time intervals to predict SOM, the best time period for predicting SOM was always within May; and (3) adding environmental covariates effectively improved the SOM mapping performance, and the multiyear average temperature was the most important factor. In general, our results demonstrated the valuable potential of SOM mapping using multiyear synthetic imagery, thereby allowing detailed mapping of large areas of cultivated soil.

**TABLE 6**
**SOC SAMPLE SET STATISTICS FOR EACH S2BSOIL USED FOR MODELLING**

| SOC g.kg−1 | | | | | | | | | | |
|---|---|---|---|---|---|---|---|---|---|---|
| **S2Bsoil** | **Sites** | **Minimum** | **Q1** | **Median** | **Mean** | **Q3** | **Maximum** | **SD** | **Skewness** | **Kurtosis** |
| S2Bsoil_0 | 353 | 3.46 | 11.4 | 13 | 13.4 | 15 | 27.8 | 3.3 | 0.86 | 4.83 |
| S2Bsoil_1 | 304 | 3.46 | 11.41 | 13 | 13.4 | 15 | 27.8 | 3.3 | 0.93 | 5.18 |
| S2Bsoil_2 | 350 | 3.46 | 11.39 | 13 | 13.4 | 15 | 27.8 | 3.3 | 0.85 | 4.82 |

Urbina-Salazar et al analysed Sentinel-2 and Sentinel-1 bare soil temporal mosaics of 6-year periods for soil organic carbon content mapping in Central France. To generate a reliable SOC map, this study addresses the use of Sentinel-2 (S2) temporal mosaics of bare soil (S2Bsoil) over 6 years jointly with soil moisture products (SMPs) derived from Sentinel 1 and 2 images, SOC measurement data and other environmental covariates derived from digital elevation models, lithology maps and airborne gamma-ray data. In this study, we explore (i) the dates and periods that are preferable to construct temporal mosaics of bare soils while accounting for soil moisture and soil management; (ii) which set of covariates is more relevant to explain the SOC variability. From four sets of covariates, the best contributing set was selected, and the median SOC content along with uncertainty at 90% prediction intervals were mapped at a 25-m resolution from quantile regression forest models. The accuracy of predictions was assessed by 10-fold cross-validation, repeated five times. The models using all the covariates had the best model performance. Airborne gamma-ray thorium, slope and S2 bands (e.g., bands 6, 7, 8, 8a) and indices (e.g., calcareous sedimentary rocks, "calcl") from the "late winter–spring" time series were the most important covariates in this model. Our results also indicated the important role of neighbouring topographic distances and oblique geographic coordinates between remote sensing data and parent material. These data contributed not only to optimizing SOC mapping performance but also provided information related to long-range gradients of SOC spatial variability, which makes sense from a pedological point of view.

### 2.3 Soil Salinity:

Meti et al carried-out sensitivity analysis for mapping of alkaline soil in Northern Dry Zone of Karnataka, India using Sentinel-1 and Landsat-8 bands. This paper focuses on exploring the possibility of using new generation medium resolution Landsat-8 and Sentinel-2 satellite data to map alkaline soils of Ramthal irrigation project area in north Karnataka. Surface soil salinity parameters of zone 20 were correlated with reflectance values of different band and band combination and traditional salinity indices and result has indicated that SWIR bands of both satellites showed significant negative correlation with soil pH, EC (r=-0.39 to - 0.45) whereas visible and NIR bands did not show significant relation. However, rationing of SWIR bands with visible blue band has significantly improved the correlation with soil pH and EC (r= +0.60 to +0.70). Traditional salinity index based on visible bands failed to show significant correlation with soil parameters. It is interesting to note that SWIR bands alone did not show significant correlation with soil sodicity parameters like exchangeable Na, SAR, RSC but band rationing with blue bands has significantly improved the correlation (r = 0.45). High resolution soil salinity map was prepared using simple linear regression model and using this map will serve as base map for the policy makers.

**TABLE 7**
**LINEAR REGRESSION MODELS FOR PREDICTING SOIL SALINITY PARAMETERS FROM SATELLITE BANDS REFLECTANCE**

| Parameter | Satellite | Regression Model | $R^2$ | RMSE |
|---|---|---|---|---|
| pH | Landsat 8 | 6.41+15.73(Aerosol/SWIR2) + 4.95(Green/NIR) -11.69 (Blue/SWIR1) | 0.48 | 0.207 |
| | Sentinel 2 | 7.17+8.72((Blue/SWIR2) +1.87(RedEdge2/RedEdge3)-5.44(SI7)-1.0(Blue/RedEdge1) | 0.49 | 0.206 |
| EC | Landsat 8 | 0.09+2.02(Aerosol/SWIR2) +0.67(Red/NIR)-7.35(Blue)-0.34(Blue/Green) | 0.33 | 0.07 |
| | Sentinel 2 | 0.17-0.94(SWIR2) +1.13(RedEdge1/SWIR1) +1.13(SI7) | 0.3 | 0.07 |
| Sodium | Landsat8 | -17.04+144.29(Aerosol/SWIR2) +45.66(Green/NIR)-132.28(Blue/SWIR1) | 0.49 | 1.51 |
| | Sentinel 2 | -1.59-51.1(SWIR2) +36.39((Blue/SWIR1) +17.28(Green/NIR) | 0.45 | 1.58 |

Ghada investigated a PLSR model to predict soil salinity using Sentinel-2 MSI data. This study used spectral indices, including salinity and vegetation indices, Sentinel-2 MSI original bands, and DEM, to model soil salinity in the Great Hungarian Plain. Eighty-one soil samples in the upper 30 cm of the soil surface were collected from vegetated and non vegetated areas by the Research Institute for Soil Sciences and Agricultural Chemistry (RISSAC). The sampling campaign of salinity monitoring was performed in the dry season to enhance salt spectral characteristics during its accumulation in the subsoil. Hence, applying a partial least squares regression (PLSR) between salt content (g/kg) and remotely sensed data manifested a highly moderate correlation with a coefficient of determination $R^2$ of 0.68, a p-value of 0.000017, and a root mean square error of 0.22. The final model can be deployed to highlight soil salinity levels in the study area and assist in understanding the efficacy of land management strategies.

**TABLE 8**
**MULTIPLE LINEAR REGRESSION ANALYSIS – ECp VERSUS LABORATORY ANALYSED SOIL ECe**

| | | RMSE | | MBE | |
|---|---|---|---|---|---|
| Model | $R^2$ | (dS $m^{-1}$) | (%) | (dS $m^{-1}$) | (%) |
| 1 | 0.44* | 1.09 | 14.34 | 1.25 | –17.29 |
| 2 | 0.54* | 0.94 | 10.61 | 1.08 | –14.22 |
| 3 | 0.62* | 0.86 | 10.02 | 0.92 | 6.66 |

Khalid et al used Sentinel-2 images for effective mapping of soil salinity in agricultural fields. The present study was conducted to develop an effective soil salinity prediction model using Sentinel2A (S2) satellite data. Initially, the collected soil samples were analysed for soil salinity (ECe). Subsequently, multiple linear regression analysis was carried out between the obtained ECe values and S2 data, for the prediction of soil salinity models. The relationship between ECe and S2 data, including individual bands, band ratios and spectral indices showed moderate to highly significant correlations ($R^2$ = 0.43–0.83). A combination of SWIR-1 bands and the simplified brightness index was found to be the most appropriate ($R^2$ = 0.65; $P < 0.001$) for prediction of soil salinity. The results of this study demonstrate the ability to obtain reliable estimates of EC using S2 data.

Sameh studied Sentinel-2 based mapping of soil salinity of arid soils in southeastern regions of Tunisia. In this study, 80 samples were collected from the soil surface (the upper 10 cm). A predictive model was constructed based on the measured soil electrical conductivity (EC) and spectral indices developed from satellite image. The results revealed that salinity index SI1, SI2 and band 3 have the highest correlation with EC. Multiple regression analysis showed a moderate accuracy with $R^2$ = 0.42 and an RMSE = 18.3.

**TABLE 9**
**MULTIPLE REGRESSION MODEL BETWEEN SPECTRAL INDICES AND MEASURED EC**

| Regression model | $R^2$ | RMSE |
|---|---|---|
| EC= - 109.92-0.1b4 + 0.08b2-0.03b3-0.03SI2 + 0.07b8-0.05b6 + 0.03SI1 | 42% | 18.3ds/m |

Gogumalla et al detected soil pH from open-source remote sensing data: A case study of Angul and Balangir Districts, Odisha State. The objective of this research was to estimate soil pH from Sentinel-1, Sentinel-2, and Landsat-8 satellite-derived indices; data from Sentinel-1, Sentinel-2, and Landsat-8 satellite missions were used to generate indices and as proxies in a statistical model to estimate soil pH. Step-wise multiple regression (SWMR), artificial neural networks (ANN), and random forest (RF) regression were used to develop predictive models for soil pH, SWMR, ANN, and RF regression models. The SWMR greedy method of variable selection was used to select the appropriate independent variables that were highly correlated with soil pH. Variables that were retained in the SWMR are B2, B11, Brightness index, Salinity index-2, Salinity index-5 of Sentinel-2 data; VH/VV index of Sentinel 1 and TIR1 (thermal infrared band1) Landsat-8 with p-value 0.05. Among the four statistical models developed, the class-wise RF model performed better than other models with a cumulative correlation coefficient of 0.87 and RMSE of 0.35. The better performance of class-wise RF models can be attributed to different spectral characteristics of different soil pH groups.

Kaya et al studied predictive mapping of electrical conductivity and assessment of soil salinity in a Western Turkiye, Alluvial Plain. The current study area is located in the Isparta province (100 $km^2$), land cover is mainly irrigated, and the dominant soils are Inceptisols, Mollisols, and Vertisols. Digital soil mapping (DSM) methodology was used, referring to the increase in the digital representation of soil formation factors with today's technological advances. Plant and soil-based indices produced from the Sentinel 2A satellite image, topographic indices derived from the digital elevation model (DEM), and CORINE land cover classes were used as predictors. The support vector regression (SVR) algorithm revealed the best relationships in the study area. Considering the estimates of different algorithms, according to the FAO salinity classification, a minimum of 12.36% and a maximum of 20.19% of the study area can be classified as slightly saline. The low spatial dependence between model residuals limited the success of hybrid methods. The land irrigated cover played a significant role in predicting the current level of EC.

Nada et al obtained salinity properties retrieval from Sentinel-2 satellites data and machine learning algorithms. The objective of this study was to achieve the best estimation of electrical conductivity variables from salt-affected soils in a south Mediterranean region using Sentinel-2 multispectral imagery. In order to realize this goal, a test was carried out using electrical conductivity (EC) data collected in central Tunisia. Soil electrical conductivity and leaf electrical conductivity were measured in an olive orchard over two growing seasons and under three irrigation treatments. Firstly, selected spectral salinity, chlorophyll, water, and vegetation indices were tested over the experimental area to estimate both soil and leaf EC using Sentinel-2 imagery on the Google Earth Engine platform. Subsequently, estimation models of soil and leaf EC were calibrated by employing machine learning (ML) techniques using 12 spectral bands of Sentinel-2 images. The prediction accuracy of the EC estimation was assessed by using k-fold cross-validation and computing statistical metrics. The results of the study revealed that machine learning algorithms, together with multispectral data, could advance the mapping and monitoring of soil and leaf electrical conductivity.

### 2.4 Soil Texture:

Bousbih et al estimated soil texture using radar and optical data from Sentinel-1 and Sentinel-2. The study is based on Sentinel-1 (S-1) and Sentinel-2 (S-2) data acquired between July and early December 2017, on a semi-arid area about 3000 $km^2$ in central Tunisia. In addition to satellite acquisitions, texture measurement samples were taken in several agricultural fields, characterized by a large range of clay contents (between 13% and 60%). For the period between July and August, various optical indicators of clay content Short-Wave Infrared (SWIR) bands and soil indices) were tested over bare soils. Satellite moisture products, derived from combined S-1 and S-2 data, were also tested as an indicator of soil texture. Algorithms based on the support vector machine (SVM) and random forest (RF) methods are proposed for the classification and mapping of clay content and a three-fold cross-validation is used to evaluate both approaches. The classifications with the best performance are achieved using the soil moisture indicator derived from combined S-1 and S-2 data, with overall accuracy (OA) of 63% and 65% for the SVM and RF classifications, respectively.

Gomez et al used Sentinel-2 time-series images for classification and uncertainty analysis of inherent biophysical property: Case of soil texture mapping. Two sources of uncertainty were studied: uncertainties due to the Sentinel-2 acquisition date and uncertainties due to the soil sample selection in the training dataset. The first uncertainty analysis was achieved by analysing the diversity of classification results obtained from the time series of soil texture classifications, considering that the temporal resolution is akin to a repetition of spectral measurements. The second uncertainty analysis was achieved from each individual Sentinel-2 image, based on a bootstrapping procedure corresponding to 100 independent classifications obtained with different training data. The Simpson index was used to compute this diversity in the classification results. This work was carried out in an Indian cultivated region (84 $km^2$, part of Berambadi catchment, in the Karnataka state). It used a time-series of six Sentinel-2 images acquired from February to April 2017 and 130 soil surface samples, collected over the study area and characterized in terms of texture. The classification analysis showed the following: (i) each single-date image analysis resulted in moderate performances for soil texture classification, and (ii) high confusion was obtained between neighbouring textural classes, and low confusion was obtained between remote textural classes. The uncertainty analysis showed that (i) the classification of remote textural classes (clay and sandy loam) was more certain than classifications of intermediate classes (sandy clay and sandy clay loam), (ii) a final soil textural map can be produced depending on the allowed uncertainty, and iii) a higher level of allowed uncertainty leads to increased bare soil coverage. These results illustrate the potential of Sentinel-2 for providing input for modelling environmental processes and crop management.

Yanan et al identified soil texture classes under vegetation cover based on Sentinel-2 data with SVM and SHAP techniques. multitemporal Sentinel-2 images were used to get exhaustive vegetation cover information. Basic digital elevation map (DEM) derivatives and stratum were extracted. Three support vector machines with different input parameters (purely DEM derivatives and stratum, purely Sentinel-2, and Sentinel-2 plus DEM derivatives and stratum) were developed. Moreover, in order to improve the transparency in black box ML models, the novel SHapley Additive explanations (SHAP) method was applied to interpret the outputs and analyse the importance of individual variables. Results showed that the model with all variables provided desirable performance with overall accuracy of 0.8435, F1-score of 0.835, kappa statistic of 0.7642, precision of 0.8388, recall of 0.8355, and area under the curve of 0.9451. The model with purely Sentinel-2 data performed much better than that with solely DEM derivatives and stratum. The contributions of Sentinel-2 data to explain soil texture class variability were about 17%, 41%, and 28% for sandy, loamy, and clayey soils, respectively. The SHAP method visualized the decision process of ML and indicated that elevation, stratum, and red-edge factors were critical variables for predicting soil texture classes. This study offered much-needed insights into the applications of Sentinel-2 data in digital soil mapping and ML-assisted tasks.

Miao et al mapped soil texture in Songnen plain of China using sentinel-2 imagery. For this study collecting 354 topsoil (0–20 cm) samples in Songnen plain and evaluating the effectiveness of the bands and spectral indices of Sentinel-2 images and RF algorithm in predicting soil texture (sand, silt, and clay fractions). The results demonstrated that the 16 covariates were moderately and highly correlated with soil texture. And, Band11 of Sentinel-2 images could be used as the corresponding band of soil texture. For sand fraction, the Sentinel-2 images and RF algorithm's Coefficient of Determination ($R^2$) and Root Mean Square Error (RMSE) were 0.77 and 10.48%, respectively, and for silt fraction, they were 0.75 and 9.38%. Sand fraction decreased from southwest to northeast in Songnen plain, while silt and clay fractions increased. We found that the Songnen Plain was affected by water erosion and wind erosion, in the northeast and southwest, respectively, providing reference for the implementation of Conservation Tillage policies. The outcome of the study can provide reference for future soil texture mapping with a high resolution.

### 2.5 All Soil Properties

Vaudour et al studied Sentinel-2 image capacities to predict common topsoil properties of temperate and Mediterranean agroecosystems. Prediction models of soil properties based on partial least squares regressions (PLSR) were built from S2A spectra of 72 and 143 sampling locations across the Versailles Plain and Peyne catchment, respectively. Eight soil surface properties were investigated in both regions: pH, cation exchange capacity (CEC), texture fractions (Clay, Silt, Sand), Iron, Calcium Carbonate ($CaCO_3$) and Soil Organic Carbon (SOC) content. Predictive abilities were studied according to the root mean square error of cross-validation (RMSECV) tests, cross-validated coefficient of determination ($R^2$ cv) and ratio of performance to deviation (RPD). Intermediate prediction performance outcomes ($R^2$ cv and RPD greater than or equal to 0.5 and 1.4, respectively) were obtained for 4 topsoil properties found across the Versailles Plain (SOC, pH, $CaCO_3$ and CEC), and near-intermediate performance outcomes ($0.5 > R^2$ cv $> 0.39$, $1.4 >$ RPD $> 1.3$) were yielded for 3 topsoil properties (Clay, Iron, and CEC) found across the Peyne catchment and for 1 property (Clay) found across the Versailles Plain. The study results show what can be expected from Sentinel-2 images in terms of predictive capacities at the regional scale. The spatial structure

of the estimated soil properties for bare soils pixels is highlighted, promising further improvements made to spatial prediction models for these properties based on the use of Digital Soil Mapping (DSM) techniques.

Santaga et al used sentinel-2 for simplifying soil sampling and mapping: Two case studies in Umbria, Italy. This study developed and tested a streamlined soil mapping methodology, applicable at the field scale, based on an unsupervised classification of Sentinel-2 (S2) data supporting the definition of reduced soil-sampling schemes. The study occurred in two agricultural fields of 20 hectares each near Deruta, Umbria, Italy. S2 images were acquired for the two bare fields. After a band selection based on bibliography, PCA (Principal Component Analysis) and cluster analysis were used to identify points of two reduced sample schemes. The data obtained by these samplings were used in linear regressions with principal components of the selected S2 bands to produce maps for clay and organic matter (OM). Resultant maps were assessed by analysing residuals with a conventional soil sampling of 30 soil samples for each field to quantify their accuracy level. Although of limited extent and with a specific focus, the low average errors (Clay ± 2.71%, OM ± 0.16%) we obtained using only three soil samples suggest a wider potential for this methodology. The proposed approach, integrating S2 data and traditional soil-sampling methods could considerably reduce soil-sampling time and costs in ordinary and precision agriculture applications.

Yuvaraj et al performed spectral indices for soil properties: a case study from Redland farm, south Florida. In this work, they explore the capabilities of multispectral images (Sentinel 2A and Landsat 8) for accessing the dynamic soil properties of the study site. The predefined combinations of spectral band values (spectral indices) of Sentinel 2A and Landsat 8 image on the study area were used for evaluation. The correlation coefficient and linear regression models were demonstrated to assess the relationship between the derived spectral indices and five topsoil properties (Bulk Density (BD), Soil Organic Matter (SOM), Electric Conductivity (EC), pH, and Water Content). The results illustrated that specific soil properties (SOM, EC, pH, and BD) correlated well with different spectral indices with both images. Eight spectral bands combinations were found good with three soil properties with maximum correlation coefficient (R=0.623) for Sentinel 2A, and Landsat 8 has maximum correlation coefficient (R=0.463) of three spectral indices for two soil properties. The influence of distinct spectral bands of multispectral satellite images in soil surface properties involved in the best-suited indices algorithms was discussed in this article. Overall, we found that the spectral indices demonstrated promising results for this study, and hence they can be accounted for in soil investigation in agriculture.

Piccoli et al estimated multiple soil characteristics of a continental-wide area corresponding to the European region, using multispectral Sentinel-3 satellite imagery and digital elevation model (DEM) derivatives. The results confirm the importance of multispectral imagery in the estimation of soil properties and specifically show that the use of DEM derivatives improves the quality of the estimates, in terms of $R^2$, by about 19% on average. In particular, the estimation of soil texture increases by about 43%, and that of cation exchange capacity (CEC) by about 65%. The importance of each input source (multispectral and DEM) in predicting the soil properties using machine learning has been traced back. It has been found that, overall, the use of multispectral features is more important than the use of DEM derivatives with a ration, on average, of 60% versus 40%.

## III. CONCLUSION

The study concluded that many researchers worked on estimating soil properties using sentinel-1, Sentinel-2 and Sentinel-3 satellite data. In which according to the various researcher's sentinel-2 data provide maximum accuracy during estimation of various properties along with various model.

## REFERENCES

[1] Barnes E, Baker M. 2000. Multispectral data for mapping soil texture: Possibilities and limitations. *Applied Engineering Agriculture* **16**(5)**:**731–741.

[2] Bousbih S, Mehrez Z, Charlotte P, Azza G, Zohra L, Nicolas B, Nadhira B and Bernard M.2019. Soil Texture Estimation Using Radar and Optical Data from Sentinel-1 and Sentinel-2. *Remote Sensing* **11**(1520):1-20.

[3] Castaldi F, Chabrillat S, Don A and Wesemael B.2019. Soil Organic Carbon Mapping Using LUCAS Topsoil Database and Sentinel-2 Data: An Approach to Reduce Soil Moisture and Crop Residue Effects. *Remote Sensing* **11**(21):2121.

[4] Castaldi F, Chabrillat S, and Wesemael B.2019.Sampling Strategies for Soil Property Mapping Using Multispectral Sentinel-2 and Hyperspectral EnMAP Satellite Data. *Remote Sensing*, **11**(3).

[5] Chong L, Wenqi Z, Xinle Z, and Huanjun L.2023.Mapping Soil Organic Matter Content Using Sentinel-2 Synthetic Images at Different Time Intervals in Northeast China, *International Journal of Digital Earth*, **16**(1):1094-1107.

[6] Dematte J, Huete A, Ferreira L, Nanni M, Alves M and Fiorio P.2009. Methodology for bare soil detection and discrimination by Landsat TM image. *The Open Remote Sensing Journal* **2**(1): 24–35.

[7] Esmaeili S, Sahebi V, and Jazirian I. 2022. Estimation of Soil Moisture using Sentinel-1 and Sentinel-2 Images. ISPRS Annals of the Photogrammetry, *Remote Sensing and Spatial Information Sciences* **4**:137-145.

[8] Flavio P, Mirko B, Marco P, and Paolo N.2023. Estimation of Soil Characteristics from Multispectral Sentinel-3 Imagery and DEM Derivatives Using Machine Learning. *Sensors* **23**(15):7876.

[9] Ghada S.2021. A PLSR Model to Predict Soil Salinity Using Sentinel-2 MSI data. *Open geosciences* **13**(1):977-987.

[10] Gogumalla P, Rupavatharam S, Datta A, Khopade R, Choudhari P, Dhulipala R and Dixit S.2022. Detecting Soil pH from Open-Source Remote Sensing Data: A Case Study of Angul and Balangir Districts, Odisha State. *Journal of the Indian Society of Remote Sensing* 1-16.

[11] Gomez C, Subramanian D, Jean-Baptiste F, Philippe L, Laurent R and Muddu S.2019. Use of Sentinel-2 Time-Series Images for Classification and Uncertainty Analysis of Inherent Biophysical Property: Case of Soil Texture Mapping. *Remote Sensing* **11**(565):1-28.

[12] Helfer G, Barbosa J, Alves D, da Costa A, Beko M and Leithardt, V.2021. Multispectral Cameras and Machine Learning Integrated into Portable Devices as Clay Prediction Technology. *Journal of Sensor and Actuator Networks*. **10**(40):1-12.

[13] Jaroslav N, Vojtech L and Jan K.2018.Estimation of Soil Properties Based on Soil Colour Index. *Agriculturae Conspectus Scientificus* **83**(1):71-76.

[14] Kaya F, Schillaci C, Keshavarzi A and Basayigit L.2022. Predictive Mapping of Electrical Conductivity and Assessment of Soil Salinity in a Western Türkiye Alluvial Plain. *Land* **11**(2148):1-21.

[15] Khalid A, ElKamil, Rangaswamy M, and Ronnel B. 2021. Sentinel-2 images for effective mapping of soil salinity in agricultural fields. *Current Science* **121**(3):384-390.

[16] Klara D, Uta H, Karin P, Gijs S, and Gera V, and Basvan W. 2022. Improving soil organic carbon predictions from a Sentinel–2 soil composite by assessing surface conditions and uncertainties. *Geoderma*.**4**(29):116-128.

[17] Lagacherie P, Baret F, Feret J, Netto Jand Robbez-Masson, J.2008. Estimation of soil clay and calcium carbonate using laboratory, field, and airborne hyperspectral measurements. *Remote Sensing of Environment* **112**(3):825–835.

[18] Madugundu R, Al-Gaddi K, Tola E, Edris M, Edrees H, Alameen A and Fulleros R.2021. Estimation of soil organic carbon in agricultural fields: A remote sensing approach. *Journal of Environmental Biology* **43**(1):73-84.

[19] Mammadov E, Denk M, Riedel F, Lewinski K, Kaźmierowski C, and Glaesser C.2020. Visible and near-infrared reflectance spectroscopy for assessment of soil properties in the Caucasus Mountains, Azerbaijan. *Communications in Soil Science and Plant Analysis* **51**(17): 2111–2136.

[20] Meti S, Hanumesh P, Lakshmi M, Nagaraja S and Shreepad V. 2019.Sentinel 2 and landsat-8 bands sensitivity analysis for mapping of alkaline soil in northern dry zone of karnataka, India. *ISPRS-archives* **XLII-3**(W6) :307.

[21] Miao Z, Xiang W, Sijia L, Bingxue Z, Junbin H and Kaishan S.2023. Soil Texture Mapping in Songnen Plain of China Using Sentinel-2 Imagery. *Remote Sensing***15**(5331):1-14.

[22] Nada M, Olfa B, Rossella A, Anna S, Mohamed B and Mladen T.2023. Salinity Properties Retrieval from Sentinel-2 Satellite Data and Machine Learning Algorithms **13**(1):1-18.

[23] Natalia E, Mohamed E, and Esra E.2021. Soil Moisture Estimation using Sentinel-1/-2 Imagery Coupled with cycleGAN for Time-series Gap Filing. *IEEE transactions on geoscience and remote sensing* **XX**:1-11.

[24] Paloscia S, Pettinato S, Santi E, Notarnicola C, Pasolli L and Reppucci A.2013. Soil moisture mapping using Sentinel-1 images: Algorithm and preliminary validation. *Remote Sensing of Environment* **134**(1):234-248.

[25] Peng Y, Zhao L, Hu Y, Wang G, Wang L, and Liu Z.2019. Prediction of soil nutrient contents using visible and near-infrared reflectance spectroscopy. *ISPRS International Journal of Geo-Information* **8**(1):29.

[26] Piccoli F, Barbato M, Peracchi M and Napoletano P.2023. Estimation of Soil Characteristics from Multispectral Sentinel-3 Imagery and DEM Derivatives Using Machine Learning. *Sensors* **23**(15):7876.

[27] Qi G, Mehrez Z, Maria J, Escorihuela and Baghdadi N.1966. Synergetic use of Sentinel-1 and Sentinel-2 data for soil moisture mapping at 100 m resolution. *Sensors* **17**(1):1-21.

[28] Sameh H, Houda S and Abbelhakim B.2022. Sentinel-2 based mapping of soil salinity of arid soils in southeastern regions of Tunisia. *Research Square*.

[29] Santaga .F, Alberto A, Angelo L and Marco V.(2021). Using Sentinel-2 for Simplifying Soil Sampling and Mapping: Two Case Studies in Umbria, Italy. *Remote Sensing* **13**(3379):1-15.

[30] Santaga F, Agnelli A, Leccese A and Vizzari M.2021.Using Sentinel-2 for Simplifying Soil Sampling and Mapping: Two Case Studies in Umbria, Italy. *Remote Sensing* **13**(16):3379.

[31] Sutariya S, Hirapara A, Meherbanali M, Tiwari M, Singh V, and Kalubarme M.2021.Soil Moisture Estimation Using Sentinel-1 Sar Data and Land Surface Temperature in Panchmahal District, Gujarat State. *International Journal of Environment and Geoinformatics* **8**(1):065-077.

[32] Toth G, Jones A and Montanarella L.2013. The LUCAS topsoil database and derived information on the regional variability of cropland topsoil properties in the European Union Environment . *Environmental Monitoring and Assessment* **185**(7): 4487-4504.

[33] Urbina-Salazar D, Vaudour E, Richer-de-Forges A, Chen S, Martelet G, Baghdadi N and Arrouays D.2023. Sentinel-2 and Sentinel-1 Bare Soil Temporal Mosaics of 6-Year Periods for Soil Organic Carbon Content Mapping in Central France. *Remote Sensing* **15**(9):2410.

[34] Vaudour E, Gomez C, Fouad Y and Lagacherie P.2019. Sentinel-2 image capacities to predict common topsoil properties of temperate and Mediterranean agroecosystems. *Remote Sensing of Environment* **223**:21-33.

[35] Wang D and Shang Y. 2014. A New Active Labelling Method for Deep Learning. *Proceedings in 2014 International Joint Conference on Neural Networks (IJCNN)*. pp 112–119. 6–11 July 2014. Beijing, China.

[36] Xinxin W, Jigang H, Xia W, Huaiying Y, and Lang. Z. 2021. Estimating Soil Organic Matter Content Using Sentinel-2 Imagery by Machine Learning in Shanghai. *IEEE Access* **9** :78215-78225.

[37] Yanan Z, Wei W, Huan W, Xin Z, Chao Y, and Hongbin L.2022.Identification of Soil Texture Classes Under Vegetation Cover Based on Sentinel-2 Data with SVM and SHAP Techniques. *IEEE journal of selected topics in applied earth observations and remote sensing***15(8)** :3757-3770.

[38] Yuvaraj D, Jayachandran K and Ashokkumar L.2022. Performance of spectral indices for soil properties: A case study from Redland farm, south Florida. Modelling Earth Systems and Environment **8**(1):139-150.

[39] Yuzugullu O, Lorenz F, Frohlich P and Liebisch F.2020.Understanding Fields by Remote Sensing: Soil Zoning and Property Mapping. *Remote Sensing* **12**(11):16.